Supporting Information

Picomolar zinc binding modulates formation of Bcl10-nucleating assemblies of the caspase recruitment domain (CARD) of CARD9

Michael J. Holliday, Ryan Ferrao, Gladys de Leon Boenig, Alberto Estevez, Elizabeth Helgason, Alexis Rohou, Erin C. Dueber, Wayne J. Fairbrother

Supporting information contains supporting figures S1-S7.

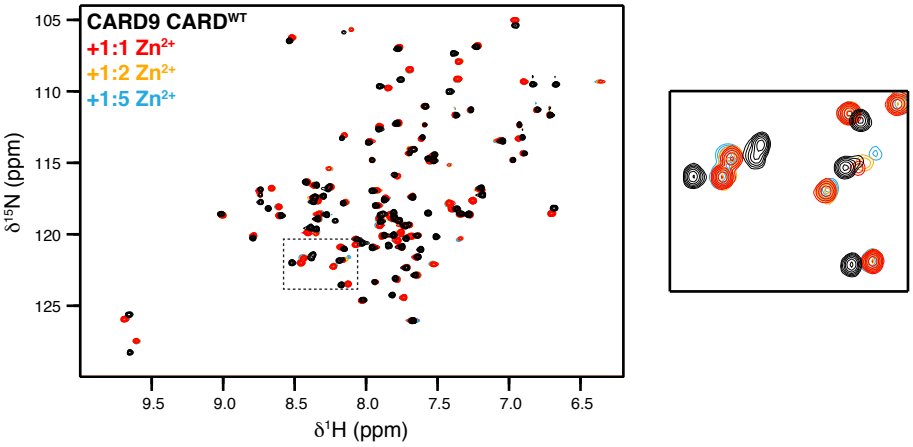

Figure S1. Low affinity, non-specific interactions between the CARD9 CARD and Zn^{2+} at concentrations above a 1:1 ratio. ^{15}N-HSQC spectra of CARD9 CARD^{WT} with 1:0 (black), 1:1 (red), 1:2 (orange), and 1:4 (blue) Zn^{2+}. Selected region indicated by dashed-line box is expanded on the right.

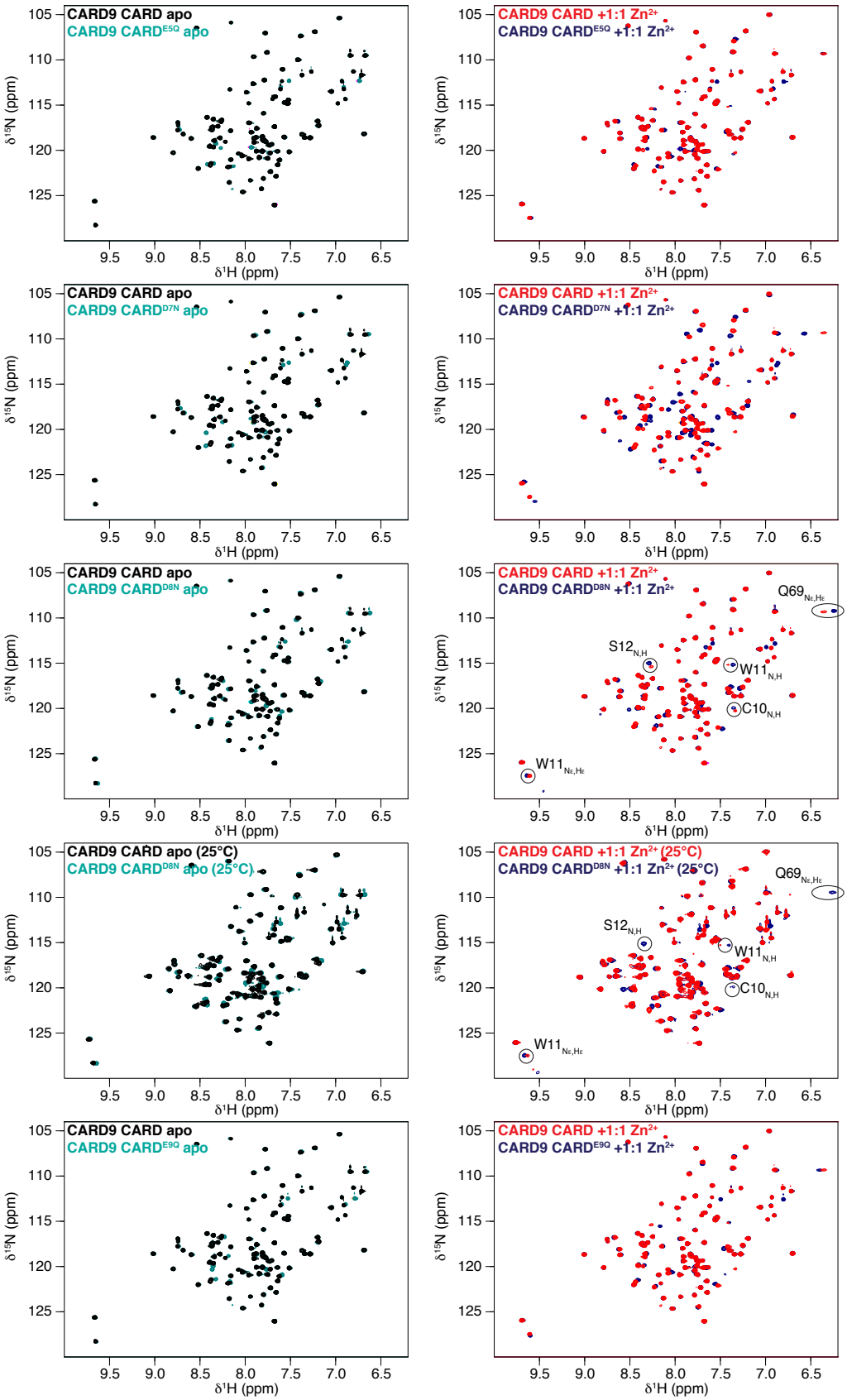
CARD9 CARD apo
CARD9 CARD^{E5Q} apo
CARD9 CARD +1:1 Zn^{2+}
CARD9 CARD^{E5Q} +1:1 Zn^{2+}
CARD9 CARD^{D7N} apo
CARD9 CARD^{D7N} +1:1 Zn^{2+}
CARD9 CARD^{D8N} apo
CARD9 CARD^{D8N} +1:1 Zn^{2+}
$Q69_{N\varepsilon,H\varepsilon}$
$S12_{N,H}$
$W11_{N,H}$
$C10_{N,H}$
$W11_{N\varepsilon,H\varepsilon}$
CARD9 CARD apo (25°C)
CARD9 CARD^{D8N} apo (25°C)
CARD9 CARD +1:1 Zn^{2+} (25°C)
CARD9 CARD^{D8N} +1:1 Zn^{2+} (25°C)
CARD9 CARD^{E9Q} apo
CARD9 CARD^{E9Q} +1:1 Zn^{2+}
$\delta^{15}N$ (ppm)
$\delta^{1}H$ (ppm)

Figure S2. Asp7 and Asp8 are involved in Zn^{2+} coordination. ^{15}N-HSQC spectra of CARD9 $CARD^{WT}$ (black/red) overlaid with $CARD^{E5Q}$, $CARD^{D7N}$, $CARD^{D8N}$, or $CARD^{E9Q}$ (green/navy). Spectra on the left are of the apo form, spectra on the right are in the presence of equimolar $ZnCl_2$. Unless indicated, all spectra were collected at 37°C. For CARD9 $CARD^{D8N}$ in the Zn^{2+}-bound state, some linewidth changes as compared to CARD9 $CARD^{WT}$ are more readily apparent at 25°C, so spectra are shown both at 37°C and 25°C. Peaks for which significant linewidth differences were identified have been circled and labeled.

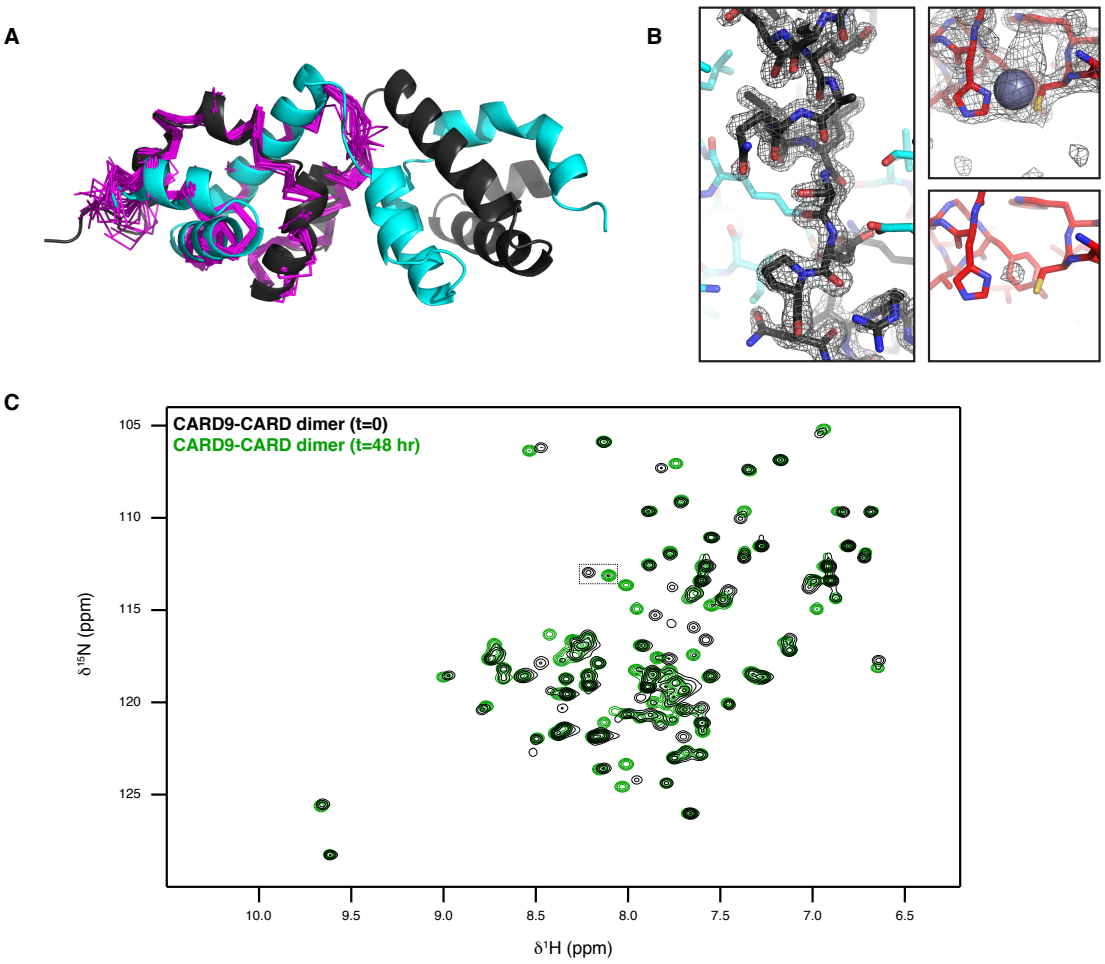

Figure S3. (A) Alignment of one half of the CARD9-CARD dimer (gray and cyan) with the 20 lowest energy structures of the monomeric apo CARD9-CARD solution structure (magenta). (B) (left) $2F_O$-F_C electron density map contoured to 1.5σ and atomic model of the apo CARD9-CARD dimer with the two chains in gray and cyan, demonstrating unambiguous density in the backbone linking helices α3 and α4 in the domain-swapped dimer. (right) Zn^{2+}-binding site in the Zn^{2+}-bound domain-swapped dimer, with $2F_O$-F_C map contoured to 1.0σ (top) and 5.0σ (bottom, with modeled Zn^{2+} ion hidden to allow for visualization of the electron density), demonstrating the presence of Zn^{2+} in the site. (C) ^{15}N-HSQC spectrum of the CARD9-CARD domain-swapped dimer at t=0 (black), and after 48 hours at 25°C (green). Dotted line indicates the region of the spectrum plotted in Figure 5D.

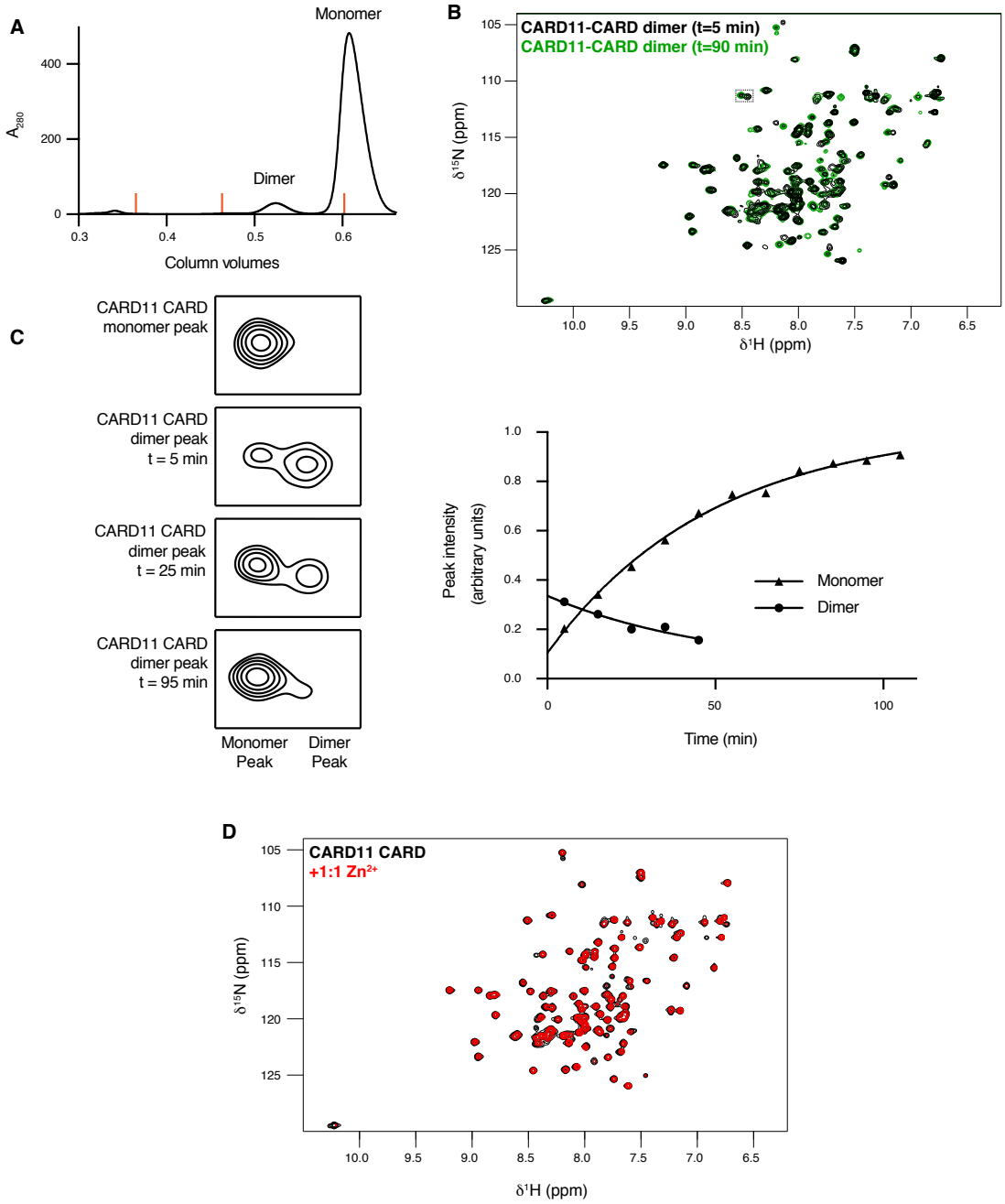

Figure S4. The CARD11 CARD adopts a dimeric form with a 34 min half-life. (A) Size exclusion chromatography UV trace (280 nm) of the CARD11 CARD, demonstrating the monomeric and dimeric peaks. Orange lines indicate peak positions of molecular weight standards of 158 kDa, 44 kDa, and 17 kDa. (B) ^{15}N-SOFAST-HMQC of the CARD11 CARD at t=5 min (black) and t=90 min (green) at 25°C. Dotted line indicates the region of the spectrum plotted in panel C. (C) (left) CARD11-CARD peak used to track dimer-to-monomer interconversion for the monomer and dimer after 5, 25, or 95 min. (right) Monomer and dimer peak heights for ^{15}N-labeled CARD11 CARD from ^{15}N-SOFAST-HMQC spectra as a function of time. Symbols represent individual measurements, solid lines represent a single exponential fit to the entire data set. (D) ^{15}N-SOFAST-HMQC spectra of ^{15}N-labeled CARD11 CARD apo (black)

and in the presence of equimolar $ZnCl_2$ (red). Peak intensities are somewhat decreased in the $ZnCl_2$ sample, perhaps due to Zn^{2+}-mediated aggregation.

A

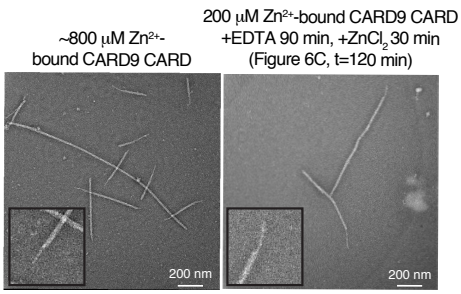

B

MBP-Bcl10	x	x	x	x	x	x	x	x	x	x	x	x	x	x	x	x	x	x
CARD9-CARD monomer							x	x	x	x	x	x						
CARD9-CARD filaments													x	x	x	x	x	x
TEV protease		x	x	x	x	x		x	x	x	x	x		x	x	x	x	x
Time (min)	10	0.5	1	2	5	10	10	0.5	1	2	5	10	10	0.5	1	2	5	10

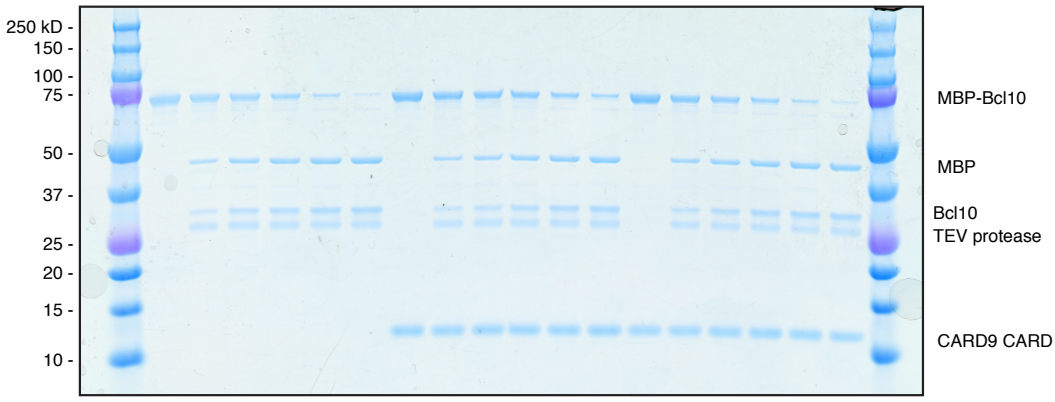

C

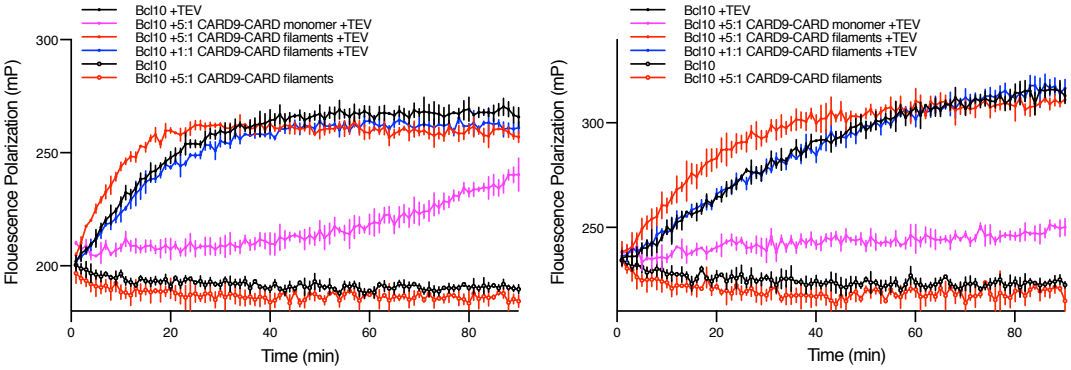

D

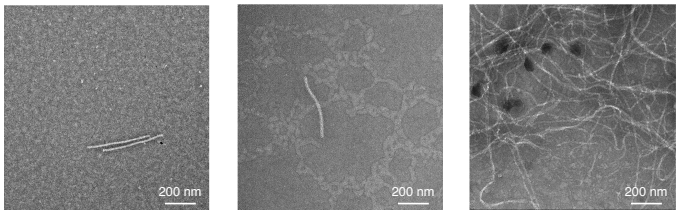

Figure S5. (A) NS-EM micrographs of (left) 1:1 Zn^{2+}-bound CARD9 CARD concentrated to ~800 μM at room temperature and (right) 200 μM 1:1 Zn^{2+} CARD9 CARD after addition of 250 μM EDTA for 90 min and subsequent addition of 250 μM $ZnCl_2$ for 30 min (endpoint of assay depicted in Figure 6C). Insets are zoomed images of selected filament termini with arrow indicating the thinner 'tails' protruding from the end. (B) Time course of MBP-Bcl10 cleavage by TEV protease alone (left columns), in the presence of 5:1 monomeric CARD9 CARD (center columns), or in the presence of 5:1 filamentous CARD9 CARD (right columns). Cleavage was carried out under identical conditions to the FP assay depicted in Figure 6E. (C) Replicate of the FP assay depicted in Figure 6E. Assay was performed identically as in Figure 6E (left) or with 1 μM (right) MBP-Bcl10, but with an independent induction of CARD9-CARD filaments and independent purification and labeling of MBP-Bcl10. For 1 μM MBP-Bcl10 assay, CARD9-CARD concentrations were adjusted to maintain the indicated stoichiometries, but TEV protease was added at the same concentration as for 2 μM. (D) Representative NS-EM micrographs of MBP-Bcl10 2 minutes after addition of TEV (left, identical grid as Figure 6F), at 90 min in the absence of TEV (center, endpoint of FP assay in Figure 6E), or at 90 min after addition of TEV (right, endpoint of FP assay in Figure 6E). Uncleaved MBP-Bcl10 filaments after 90 minutes (center) were observed much less frequently than cleaved MBP-Bcl10 filaments, even at the two-minute time point (left), consistent with the lack of an increase in FP for the uncleaved sample.

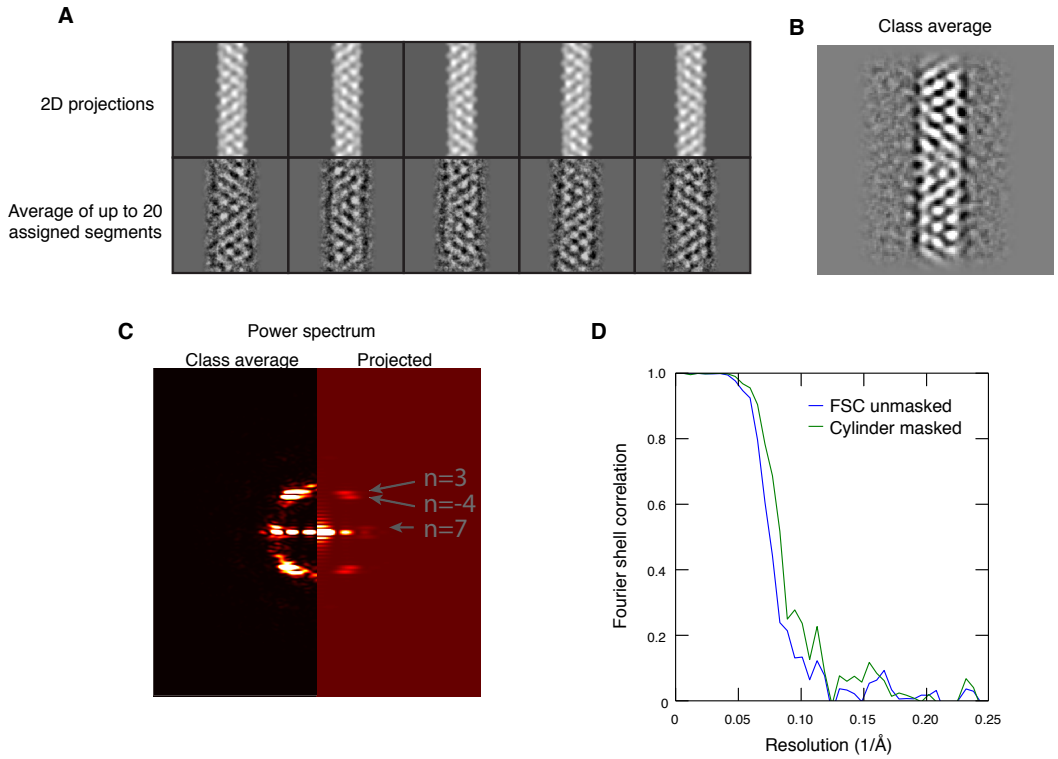

Figure S6. (A) (top) 2D projections at different azimuthal angles of the CARD9-CARD helical structure depicted in Figure 6D. (bottom) averages of up to 20 helical segments assigned to the same azimuthal angle as depicted in top row. (B) Selected class average generated for CARD9-CARD helical segments. (C) Power spectra corresponding to the class average in panel B (left) or to the corresponding 2D projection of the 3D helical reconstruction (right). Layer lines corresponding to the 3-, 4-, and 7- start helices in Figure 6D are indicated. (D) Fourier shell correlation plot for the CARD9-CARD helical assembly unmasked or masked by a cylinder of radius 100 Å. All plots were generated by Spring routines Segmentrefine3d and Segclassexam.

A

```
CARD9   1 ------------MSD-----YENDDECWSVLEGFRVTLTSVIDPSRITPYLRQCKVLNPDDEEQVLSDPNLVIRKRKVGVLLDILQRTGHKGYVAFLESLELYYPQLYKKVTGK 97
CARD11  1 MPGGGP-----EMDDYMETLKDEEDALWENVECNRHMLSRYINPAKLTPYLRQCKVIDEQDEDEVLNAPMLPSKINRAGRLLDILHTKGQRGYVVFLESLEFYYPELYKLVTGK 109
CARD10  1 MPGRAEAGEAEEEAGAGSGSEAEEDALWERIEGVRHRLARALNPAKLTPYLRQCRVIDEQDEEEVLSTYRFPCRVNRTGRLMDILRCRGKRGYEAFLEALEFYYPEHFTLLTGQ 114
CARD14  1 ------MGELCRRDS--ALTALDEETLWEMMESHRHRIVRCICPSRLTPYLRQAKVLCQLDEEEVLHSPRLTNSAMRAGHLLDLLKTRGKNGAIAFLESLKFHNPDVYTLVTGL 106
```

B

```
Human                 1 MSDYENDDECWSVLEGFRVTLTSVIDPSRITPYLRQCKVLNPDDEEQVLSDPNLVIRKRKVGVLLDILQRTGHKGYVAFLESLELYYPQLYKKVTGK 97
Chimpanzee            1 MSDYENDDECWSALEGFRVTLTSVIDPSRITPYLRQCKVLNPDDEEQVLSDPNLVIRKRKVGVLLDILQRTGHKGYVAFLESLELYYPQLYKKVTGK 97
Green monkey          1 MSDYENDDECWSVLEGFRVMLTSVIDPSRITPYLRQCKVLNPDDEEQVLSDPNLVIRKRKVGVLLDILQRTGHKGYVAFLESLELYYPQLYKKVTGK 97
Bactrian camel        1 MSDYENEDECWSALEGFRVKLIAVIDPARITPYLRQCKVLNPDDEEQVLSNPNLVIRKRKVGVLLDILQRTGHKGYVAFLESLELYYPQLYKKVTGK 97
Dog                   1 MSDYENEDQCWSTLESFRVKLISVIDPSRITPYLRQCKVLNPDDEEQVLSDPNLVIRKRKVGVLLDILQRTGHKGYVAFLESLELYYPQLYKKVTGK 97
Rat                   1 MSDYENDDECWSALESFRVKLISVIDPSRITPYLRQCKVLNPDDEEQVLSDPNLVIRKRKVGVLLDILQRTGHKGYVAFLESLELYYPQLYRKVTGK 97
Mouse                 1 MSDYENDDECWSTLESFRVKLISVIDPSRITPYLRQCKVLNPDDEEQVLSDPNLVIRKRKVGVLLDILQRTGHKGYVAFLESLELYYPQLYRKVTGK 97
Chinese hamster       1 MSDYENDDECWSALESFRVKLISVIDPSRITPYLRQCKVLNPDDEEQVLSDPNLVIRKRKVGVLLDILQRTGHKGYVAFLESLELYYPQLYRKVTGK 97
Koala                 1 MSDYENDEECWNMLESFRVKLISVIDPSRITPYLRQCKVINLDDEEQVLNDPNLVIRKRKVGVLLDILQRTGHNGYVAFLESLELYYPQLYKKVTGK 97
Duck-billed platypus 67 MSDYENDEECWNTLEGFRVKLISIIDPSRITPYLRQCKVINPDDEEQVLNDPSLVIRKRKVGVLLDILQRTGHKGYVAFLESLELYYPHLYKKITGK 163
Painted turtle       50 MSEQEDDEMCWNNLENFRVKLISVIDPSRITPYLRQCKVINHDDEEQVLNDPSLVVRKRKVGVLLDILQRTGQKGFEAFLESLELYYPQLYMKITGK 146
Chicken              32 MLEEDNDETCWNSLENFRVKLISVIDPSRITPYLRQCQVINHDDEEQVLNDPSLVMRKRKAGVLLDILQRTGRKGFEAFMESLELYYPQLYKKITGK 128
Western clawed frog   1 -MSEEEDEVCWTKLERYRVKLITVIDPNRITPYLRQCRVLNSDDEEQVFNDPNLVIRKRKVGVLLDILQRTGCKGYVAFLESLELYYPHLYKKITGS 96
Zebrafish             7 VFEVEEDDECWARLEDYRMLLIKTIEPSRITPYLRQCKVLSSEDEEQIYNDPSLVIRRRKVGVLLDILQRTGLKGYEAFLESLELDYPDVYRKITGK 97
Australian ghostshark 3 ENEDADVEELWTSLESYRAKLTSLIEPCRITAYLRQCKVINHEDEEQIFNDPNLVIRRRKVGVLLDILQRTGKKGYIAFLESLELYYPELYKRITGQ 99
```

Figure S7. (A) Multiple sequence alignment of the CARD9 CARD with its three closest paralogues, CARD11, CARD10, and CARD14. The Zn^{2+}-coordinating residues Cys10 and His73, along with their counterparts in the other sequences, are highlighted in green. (B) Multiple sequence alignment of CARD9 orthologues in various species. Zn^{2+}-coordinating residues Cys10 and His73, along with their counterparts in the other sequences, are highlighted in green.